Neoplasma 2024; 71(5): 417–427

doi:10.4149/neo_2024_240523N232

The impact of c-Met inhibition on molecular features and metastatic potential of melanoma cells

Lucia DEMKOVA[1,*], Miroslava MATUSKOVA[1], Katarina GERCAKOVA[1], Zuzana KOZOVSKA[1], Bozena SMOLKOVA[1], Lucia KUCEROVA[1,2]

[1]*Department of Molecular Oncology, Cancer Research Institute, Biomedical Research Center, Slovak Academy of Sciences, Bratislava, Slovakia;* [2]*Translational Research Unit of the 2nd Oncology Clinic, Faculty of Medicine, Comenius University and the National Cancer Institute, Bratislava, Slovakia*

**Correspondence: lucia.demkova@savba.sk*

Received May 23, 2024 / Accepted August 29, 2024

The aberrant activation of the hepatocyte growth factor receptor (c-Met) in malignant melanoma is associated with poor prognosis, fostering tumor progression, angiogenesis, and invasiveness. While therapeutic targeting of this pathway has shown promise in several tumors, our previous findings revealed increased tumorigenicity following tyrosine kinase inhibitor SU11274 treatment. Therefore, we hypothesized that administering c-Met inhibitors may elicit distinct effects in human melanoma cells. In this study, we investigated the influence of three c-Met inhibitors, SU11274, crizotinib, and PHA665752, on molecular characteristics, tumorigenicity, and metastatic behavior in three human melanoma cell lines, M4Beu, EGFP-A375 and its metastatic variant, EGFP-A375/Rel3 (Rel3). Crizotinib and PHA665752 induced upregulation of MET proto-oncogene, receptor tyrosine kinase (MET), alongside cancer stem cell marker Prominin 1 (CD133), pluripotency marker Nanog homeobox (Nanog), and genes encoding angiogenic factors and receptors in Rel3 cells, correlating with supportive effect on tumorigenicity in vivo. The increased tumorigenicity of the Rel3 cells following the SU11274 treatment correlated with the elevated phosphorylation of Akt, p70 S6 and RSK kinases. Our results demonstrate pleiotropic changes induced by small-molecule inhibitors of receptor tyrosine kinases in melanoma cell lines.

Key words: cutaneous malignant melanoma; HGF/c-Met axis; tyrosine kinase inhibitors; stemness; pluripotency; angiogenesis

Cutaneous malignant melanoma represents a significant challenge in oncology, characterized by its aggressive nature and propensity for metastasis. Despite advancements in treatment modalities, including surgical interventions, immunotherapy, and targeted therapies, the prognosis for advanced-stage melanoma remains poor. Thus, there is a pressing need for novel therapeutic approaches to target the underlying molecular mechanisms driving melanoma progression effectively.

The hepatocyte growth factor receptor (c-Met) and its ligand hepatocyte growth factor (HGF) have been associated with tumor formation and progression to metastasis [1]. Activation of c-Met was also demonstrated in malignant melanoma, and its inhibition became an emerging therapeutic strategy [2]. The c-Met expression can be induced through different mechanisms. In normal skin, HGF is produced mainly by dermal fibroblasts. The activity of c-Met can be enhanced by elevated levels of HGF produced and released by stromal and melanoma cells in response to diverse molecular stimuli [3]. The HGF/c-Met pathway, along with its downstream signaling components, including Mitogen-activated protein kinase (MAPK), the Signal transducer of activators of transcription (STAT), Phosphatidylinositol-3-kinase (PI3K)/Protein kinase B (AKT)/mammalian target of rapamycin (mTOR) and Nuclear factor-κB (NF-κβ) acts as major oncogenic drivers, promoting cancer cell survival, motility, and proliferation [4].

Inhibitors targeting the c-Met pathway in melanoma are designed to block the abnormal activation of the c-Met receptor. Crizotinib, Tivantinib, PHA665752, and quercetin have shown potential in preclinical studies [5–8]. However, some of them have encountered resistance issues [9, 10]. They could offer new co-targeting therapeutic options for melanoma treatment [5]. Ongoing research aims to optimize their effectiveness and evaluate their clinical utility in melanoma management. Inhibitor SU11274 was suggested as an effective anti-melanoma agent capable of inhibiting the c-Met receptor and decreasing the phosphorylation of c-Met

proteins [11, 12]. The combined treatment of afatinib, an ERBB family inhibitor, and crizotinib, a c-Met/ALK inhibitor, demonstrated cytotoxic effects on cutaneous malignant melanoma cells, independent of their BRAF/NRAS mutation status [13]. Kenessey et al. [11] assessed the efficacy of c-Met inhibitor SU11274 in restraining the growth of malignant melanoma metastasis. They achieved a significant antitumor and antimetastatic effect on mouse melanoma cells HT168-M1. SU11274 treatment also decreased the proliferative capacity of the human melanoma cells and induced apoptosis in the 1–5 μM concentration range *in vitro*. Moreover, it significantly reduced the migratory capacity of melanoma cells, and treatment significantly decreased primary tumor growth and liver colony formation in SCID mice [11]. In agreement, our previous research revealed reduced proliferation in both adherent and spheroid cultures following treatment with SU11274 [14]. However, intriguingly, we observed an augmented metastatic potential and increased melanoma-initiating cells *in vivo* after SU11274 treatment [14].

The molecular changes induced by treatment with three c-Met inhibitors (crizotinib, PHA665752, and SU11274) and with the Akt inhibitor LY294002 (combined with SU11274) were investigated on three human malignant melanoma cell lines with varying metastatic potential, namely EGFP-A375 its highly metastatic aggressive variant EGFP-A375/Rel3 (Rel3), and M4Beu [14, 15]. We delve into the treatment-induced changes in cancer stem cell (CSC) and pluripotency markers expression, angiogenic capacity, tumorigenicity, and metastatic potential. We anticipate that elucidating molecular mechanisms underlying these differential responses will enhance our understanding of melanoma biology and contribute to developing more effective therapeutic strategies targeting the c-Met pathway.

Materials and methods

Cell lines and cultivation conditions. EGFP-A375 cells were prepared by retroviral transduction of the melanoma A375 cell line (ATCC® CRL-1619™) [16]. EGFP-A375/Rel3 (Rel3) represents its hypermetastatic derivative [15]. Cells were cultured in high-glucose Dulbecco's modified Eagle's medium (DMEM) (PAN Biotech, Germany) supplemented with 5% fetal bovine serum (FBS) (Sigma-Aldrich, USA), 2 mM GlutaMAX (Gibco by Life Technologies, USA). Cell line M4Beu metastatic malignant melanoma cell line (kindly provided by Dr. Bízik, CRI BMC SAS Bratislava) was cultivated in high glucose DMEM (PAN Biotech, Germany) supplemented with 10% FBS (Sigma-Aldrich, USA) and 2 mM GlutaMAX (Gibco by Life Technologies, USA), with the addition of supplements as stated above. Cells were cultivated at 37 °C with 5% CO_2.

Cell exposure. The cells were treated with 1 μM SU11274 (Sigma-Aldrich, USA), 1 μM SU11274 combined with 1 μM LY29004 (SU+LY) (LY-294002 hydrochloride; Sigma-Aldrich, USA), 0.6 μM crizotinib (Rx XALKORI® Pfizer, USA) or 0.25 μM PHA665752 (MedChem Expres, USA) for 24 h. Human HGF (Miltenyi Biotec GmbH, Germany) in a concentration of 2 ng/ml for 15 min was used to activate the HGF/c-Met signaling pathway. As the studied cell lines did not have a constitutively active c-Met, we used HGF to induce phosphorylation. Cells were treated with HGF to stimulate the c-Met signaling pathway, mimicking the activation observed in the human body. This activation allowed for the investigation of the effects of c-Met inhibitors on downstream molecular events associated with tumor progression and metastasis in a physiologically relevant context.

RNA isolation and cDNA synthesis. Total RNA was isolated using a NucleoSpin® miRNA kit Catalog #740971.50 (MACHEREY-NAGEL GmbH & Co KG, Germany). The concentration was quantified using a NanoDrop ND-1000 Spectrophotometer (Thermo Scientific, USA). RNA was reverse transcribed using a Revert Aid First Strand cDNA Synthesis Kit Catalog #K1622 (Thermo Scientific, USA) following the manufacturer's instructions.

Quantitative PCR. Gene expression analysis was performed by quantitative real-time PCR (qPCR). The β-actin (*ACTB*), hypoxanthine phosphoribosyltransferase 1 (*HPRT1*), and glyceraldehyde-3-phosphate dehydrogenase (*GAPDH*) were used as references to normalize mRNA levels. Supplementary Table S1 lists the primers used for qPCR. For all reactions, Brilliant III Ultra-Fast SYBR® Green QPCR 2x Master Mix© (Agilent Technologies, Inc., USA) with specific primers (10 pM/μl) and 100 ng of template cDNA was used. qPCR was performed on BioRad CFX96 PCR Detection System (Bio-Rad CFX96TM) using the following protocol: activation at 95 °C for 3 min, 40 cycles consisting of denaturation at 95 °C for 5 s, 10 s annealing, and polymerization at 60 °C with a plate read for 5 s at 70 °C. Analyses were performed in triplicates, and data were expressed as mean ± SD. The relative quantification of mRNA expression was done using the 2–ΔΔCt method. The REST software (Qiagen) set to default parameters was used to calculate the statistical significance of group differences [17].

Western blot. Treated cells were lysed in 1× RIPA (RIPA Buffer (10×) CST Cell Signaling Technology, Inc., USA) buffer supplemented with phosphatase (PhosSTOP, Roche, Switzerland) and protease Complete ULTRA (Roche, Switzerland) inhibitors. Adherent cells were collected by scraping and lysed with a syringe and needle. Total protein concentration was determined using the Thermo-Scientific Pierce BCA Protein Assay Kit Catalog #A55860 (Thermo-Fisher Scientific, USA). For protein analysis, lysates were mixed with 4× Laemmli sample buffer, boiled, and loaded (30 μg protein/sample) onto 8% SDS-polyacrylamide gels (Bio-Rad Laboratories, Inc., USA). Proteins were transferred to nitrocellulose membranes (Thermo Fisher Scientific, USA), blocked (with 5% nonfat milk or 5% BSA), and then incubated overnight at 4 °C with primary antibodies (Supplementary Table S2). Beta-actin was used as the loading control. Membranes were incubated with HRP-conjugated secondary antibodies

(Supplementary Table S2) and visualized using LI-COR® imaging (LI-COR®, USA). Signal intensities were quantified using ImageJ software (NIH, Bethesda, Maryland, USA), and pixel density was determined and calculated using Excel (Microsoft, USA).

Proteome profiler human phospho-kinase array. The levels of kinase phosphorylation were assessed using the Human Phospho-Kinase Array Catalog #ARY003C (R&D Systems, Inc., USA). Signal intensities were quantified using ImageJ software (NIH, Bethesda, Maryland, USA), and pixel density was determined and calculated using Excel (Microsoft, USA). Per the manufacturer's instructions, sample protein concentrations were quantified using the Pierce™ BCA Protein Assay Kit Catalog #A55860 (Thermo Scientific, USA).

Subcutaneous xenograft induction. Six-week-old athymic nude mice (Balb/c nu/nu) were used following institutional guidelines in the approved animal facility (license numbers SK PC 14011 and SK UCH 02022). Bilateral subcutaneous xenografts were induced by injecting 5×10^5 Rel3 cells in 100 µl PBS and the same with pretreated Rel3 cells (1 µM SU11274 for 7 days) (SU11274-Rel3), n=4 animals/group. Tumor growth was measured three times a week using calipers. The tumor volume was calculated using the formula for ellipsoid $V = 0.5236 \times ((\text{width} + \text{length}) / 2)^3$ [18]. Mice were euthanized when xenografts reached volume 1 cm^3 as per ethical guidelines, and tissues were preserved for further analysis.

Lung colonization test. The lung colonization test was conducted using six-week SCID/bg mice. The two groups of mice were injected intravenously into the tail vein with Rel3 cells (1×10^6 Rel3 cells in 100 µl PBS) without or with 1 µM SU11274 pretreatment (7 days). The experiment was terminated 32 days after cell administration upon the onset of disease symptoms. Animals were euthanized, and organs, along with tumor masses, were excised and analyzed using qPCR.

Tissue extraction and isolation of total RNA. Thirty mg of tissue was frozen in liquid nitrogen after resection and stored at –80 °C. Before isolation, 500 µl of lysis buffer was mixed with β-mercaptoethanol (100:1 ratio) per sample and put into M Tubes (gentleMACS)™ with the frozen tissue. The gentle MACS Dissociator was used for tissue homogenization. The excessive foam was removed by centrifugation (3 min, 600×g). Subsequently, total RNA was isolated according to manufacturer instructions using a NucleoSpin® miRNA isolation kit Catalog #740971.50 (MACHEREY-NAGEL GmbH & Co KG, Germany). Total RNA was reverse-transcribed into cDNA using the first-strand cDNA RevertAid H Minus First Strand cDNA Synthesis Kit Catalog #K1622 (Thermo Fisher Scientific Inc., USA).

Detection of lung metastases. The qPCR was used to detect the expression of the *EGFP* gene in mouse lungs as evidence for the human Rel3 cells. The C(t) for samples was calculated using the formula (35 – avgC(t) of samples), where the assay cut-off C(t) is 35. PCR conditions were described above, and primer sequences are listed in Supplementary Table S1. All analyses were performed in quadruplicates.

Ethical approval. The study was performed in the approved animal facilities (license numbers SK PC 14011 and SK UCH 02022), was approved by the institutional ethics committee and by the national competence authority (State Veterinary and Food Administration of the Slovak Republic), under registration numbers Ro 3108/14-221 and 1976/17-221 in compliance with the Directive 2010/63/EU of the European Parliament and the European Council and the Regulation 377/2012 on the protection of animals used for scientific purposes.

Statistical analysis. IBM® SPSS® Statistics software, version 23.0, was used for statistical analysis. The Student's two-sample t-test or Mann-Whitney U-test was used for hypothesis testing for the difference in means of the two groups. Differences between more than two groups were analyzed by one-way analysis of variance (ANOVA) or Kruskal-Wallis H test followed by multiple comparisons. Differences with $p<0.05$ were considered statistically significant. All analyses were performed in triplicates, and data were expressed as mean ± SD. qPCR results were evaluated using REST software as described above.

Results

In tested melanoma cell lines, we analyzed the expression levels of *MET*, CSC marker *CD133*, neural stem cell markers *Nestin (Nestin), SRY-box* 2 (*SOX2)*, a marker of pluripotency *Nanog*, and *vascular endothelial growth factors A* and *B (VEGFA* and *VEGFB)* and *vascular endothelial growth factors receptors* for related tyrosine kinases (*VEGFR1* and *VEGFR2*) focusing on their relationship with enhanced proliferation, migration, cell motility, and invasiveness.

Crizotinib and PHA665752 increase gene expression of *MET*, CSC markers, *VEGFB,* and *VEGFR2* in Rel3 cells. Our results demonstrated that the expression of *MET* in Rel3 cells significantly increased upon treatment with crizotinib and PHA665752 (Figure 1A). Additionally, the expression of CSC markers *CD133* and *Nanog* was significantly elevated, while PHA665752 significantly decreased *Nestin* expression in Rel3 cells (Figure 1A). In the EGFP-A375 cell line, *CD133* was increased more than 4-fold by PHA66552. Surprisingly, in M4Beu cells, treatment with all three inhibitors decreased the expression of *Nestin* and *SOX2*.

In the hypermetastatic Rel3 cells, stimulation with HGF led to a significant increase in *VEGFR1* and *VEGFR2* expression (Figure 1A). Furthermore, crizotinib induced *VEGFB,* while both crizotinib and PHA665752 increased *VEGFR2* expression. In the EGFP-A375 cell line, no changes caused by c-Met inhibitors were found, except for an increase in *VEGFR2* observed following treatment with crizotinib and PHA665752 (Figure 1A). In M4Beu cells, all inhibitors slightly increased the expression of *VEGFA* and *VEGFR2*, while *VEGFR1* expression was downregulated. However,

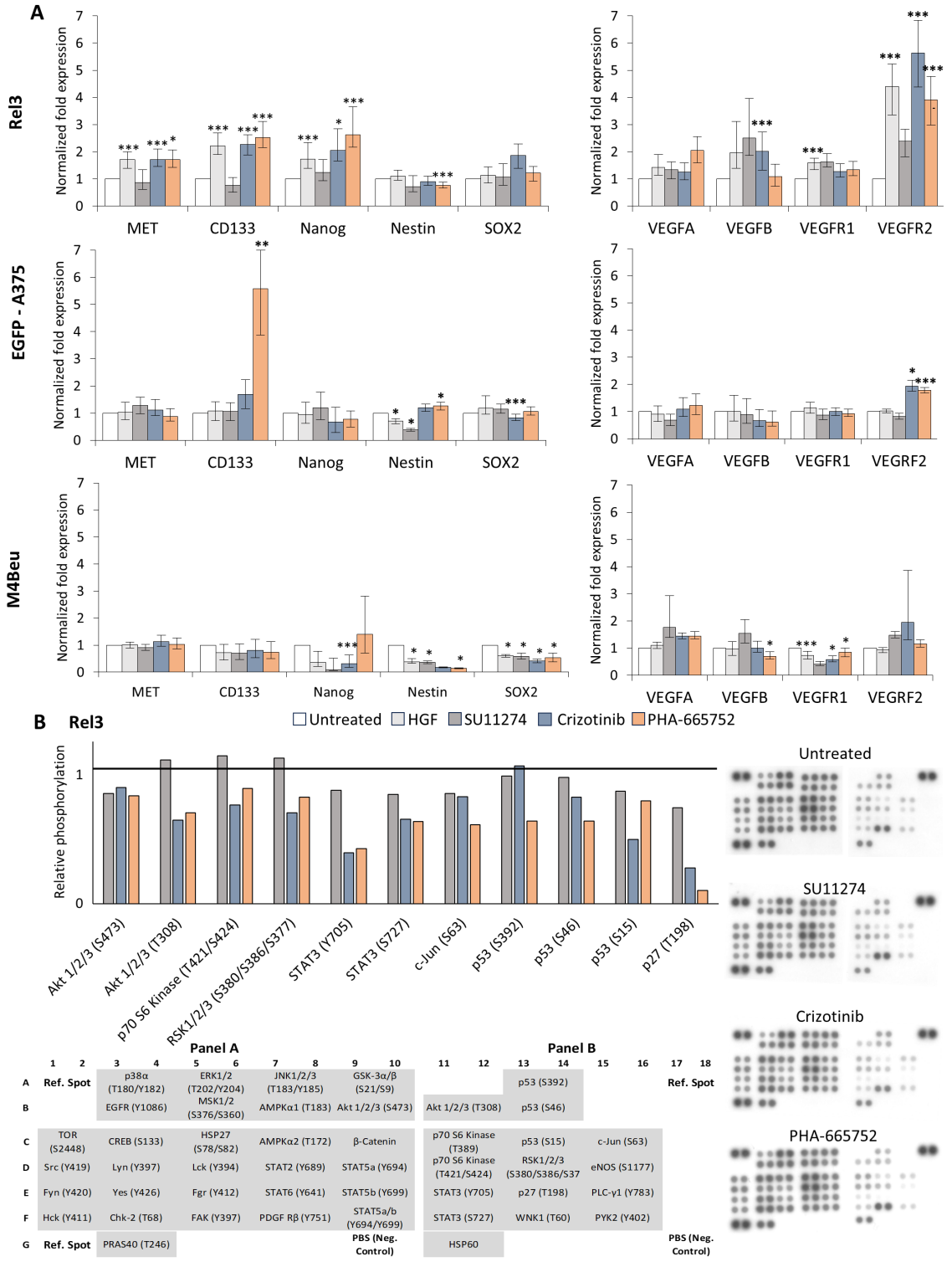

Figure 1. Gene expression changes induced by SU11274, crizotinib, and PHA665752 in Rel3, EGFP-A375, and M4Beu cell lines. A) The normalized gene expression of CSC and pluripotency markers and gene expression of the factors and receptors of vascularization and angiogenesis after treatment with inhibitors. The gene expression in all three cell lines was normalized to housekeeping genes *ACTB* and *HPRT1*; *p<0.05 and ***p<0.001. B) The phosphorylation profiles of selected intracellular proteins after inhibition with inhibitors SU11274, crizotinib, and PHA665752 in the Rel3 cell line were compared to non-treated Rel3 cells to determine the relative change in phosphorylated kinase proteins. The template with the names of the phosphorylated kinase proteins is for coordinate reference only. Part A contains 21 antibodies printed in duplicate, and Part B contains 18 antibodies printed in duplicate. Analyzed nitrocellulose membranes with the resulting spots of the array.

these changes, although significant, were mostly below the absolute fold change 2.

Impact on phosphorylation profiles of intracellular kinases and their substrates. Furthermore, we used a human phosphokinase array kit to investigate the phosphorylation profiles (Figure 1B), and the analysis revealed distinct effects of specific inhibitors on intracellular signaling molecules involved in the HGF/c-Met signaling.

Treatment with SU11274 resulted in a significant decrease in Akt (Ser473) phosphorylation, while Akt (Thr308), p70 S6 kinase (T421/S424), and RSK1/2/3 kinase were more phosphorylated. In contrast, SU11274 treatment resulted in lower phosphorylation levels of STAT3 (Tyr705 and Ser727). Additionally, using crizotinib and PHA665752, the STAT3 activation was also markedly reduced. Crizotinib and PHA665752 led to reduced phosphorylation of Akt (Thr308), p70 S6 kinase (T421/S424), and RSK1/2/3 kinase. Moreover, c-Jun (Ser63) phosphorylation was decreased in the presence of SU11274 and crizotinib, with a more pronounced reduction observed with PHA665752. Notably, phosphorylation of p53 on Ser392 and Ser46 was not suppressed by SU11274 or crizotinib. However, a slight reduction was observed at Ser15 with SU11274 and PHA665752 treatments, and a more significant decrease at Ser15 was noted with crizotinib treatment. These findings highlight the intricate and diverse effects of c-Met inhibitors on molecular pathways involved in metastasis and intracellular signaling in melanoma cells.

Impact of combination treatment with SU11274 and LY294002 on stem cell markers and angiogenic factors. Using a human phosphokinase assay, we demonstrated that SU11274 did not affect the phosphorylation of Akt (Thr308) in contrast to the other c-Met inhibitors (crizotinib and PHA665752). Based on the knowledge that LY29004 is an effective inactivator of the PI3K/AKT/mTOR signaling pathway, we decided to use it in combination with SU11274.

When SU11274 was combined with LY294002, we observed upregulation of *MET*, *Nanog*, and *SOX2* in Rel3 (Figure 2A) and *CD133* and *SOX2* in EGFP-A375 cells (Figure 2A) and in EGFP-A375 cells, treatment with SU11274 decreased *Nestin* expression. Conversely, in M4Beu cells (Figure 2A), the combination treatment reduced the expression of *CD133*, *Nestin*, and *SOX2*, while *Nanog* expression increased. Additionally, gene expression of *MET* was decreased in M4Beu cells after treatment with the SU+LY combination.

The combination treatment involving SU+LY upregulated the expression of *VEGFR1* and *VEGFR2* in Rel3 and EGFP-A375 cells (Figure 2A). This upregulation could increase vascularization and angiogenesis, essential for metastasis formation. On the contrary, in M4Beu cells, exposure to the SU+LY combination led to a significant reduction in *VEGFA* and *VEGFB* expression (Figure 2A).

Effect of c-Met inhibitors on intracellular signaling via HGF/c-Met pathway. To gain insight into the effects of c-Met inhibitors on intracellular signaling, we evaluated the inhibition of c-Met, Akt, and MAPK signaling in all studied cell lines (Figure 2B). Our aim was to ascertain if monotherapy with selected inhibitors and a combination of SU+LY could effectively suppress the phosphorylation of c-Met downstream targets, including p44/42MAPK, p38Mapk, and Akt, thereby modulating intracellular signaling. We used HGF to stimulate the c-Met protein phosphorylation.

Total c-Met protein levels remained relatively stable in treated cells, except for the combination treatment SU+LY, which showed a notable decline by half. In accordance with our expectations, we observed a specific decrease in phosphorylation of Akt (Ser473) in Rel3 (Figure 2B) cells treated with inhibitors (SU11274, crizotinib, or PHA665752), with the most significant reduction (eight-fold decrease) observed with the combination of SU+LY. All tested inhibitors effectively suppressed HGF-induced Akt phosphorylation in Rel3 cells. Notably, the PHA665752 treatment resulted in a two-fold decrease in phosphorylated p44/42 MAPK in HGF-induced Rel3 cells. Furthermore, the phosphorylation of p38 MAPK was reduced by approximately 1.5-fold after treatment with SU11274 and PHA665752, and crizotinib treatment showed a more substantial reduction (3.4-fold decrease) compared to untreated Rel3 cells.

The treatment in the EGFP-A375 cells (Figure 2B) reduced c-Met protein while increasing total p38 MAPK levels. Despite treatment, the phosphorylation status of downstream effectors such as MAPK p44/42 and p38 remained relatively high. A notable decrease in Akt (Ser473) phosphorylation was achieved with SU11274 treatment, even after HGF stimulation and also by combined treatment SU+LY. Conversely, crizotinib and PHA665752 increased Akt phosphorylation in EGFP-A375 cells.

Upon HGF stimulation of M4Beu melanoma cells (Figure 2B), phosphorylation of c-Met, p44/42 MAPK, Akt, and p38 MAPK proteins was observed, mirroring the response seen in Rel3 and EGFP-A375 cells. Treatment with SU11274 and crizotinib increased total c-Met levels but did not alter its phosphorylation status.

Despite these treatments, the phosphorylation levels of downstream effectors such as Akt, p44/42 MAPK, and p38 MAPK remained elevated. The combination of SU+LY observed a threefold decrease in Akt (Ser473) phosphorylation, consistent with findings in Rel3 and EGFP-A375 cells. However, it did not wholly inhibit Akt phosphorylation. Akt (Ser473) phosphorylation was also reduced upon PHA665752 treatment.

Tumorigenic and metastatic potential of SU11274 and LY294002 pretreated Rel3 cells *in vivo*. As we previously reported [14, 15], untreated Rel3 cells develop into tumors in organisms. In this paper, we investigated the impact of pretreatments with SU11274 and SU+LY on the tumorigenicity of the Rel3 cell line. Subcutaneous injection of the SU11274-Rel3 and SU+LY Rel3 cells results in the growth of xenotransplants (Figure 3A). Still, there was no significant difference in subcutaneous tumor growth at the end of the experiment on day 15 (1314 mm^3 vs. 1068 mm^3, respectively).

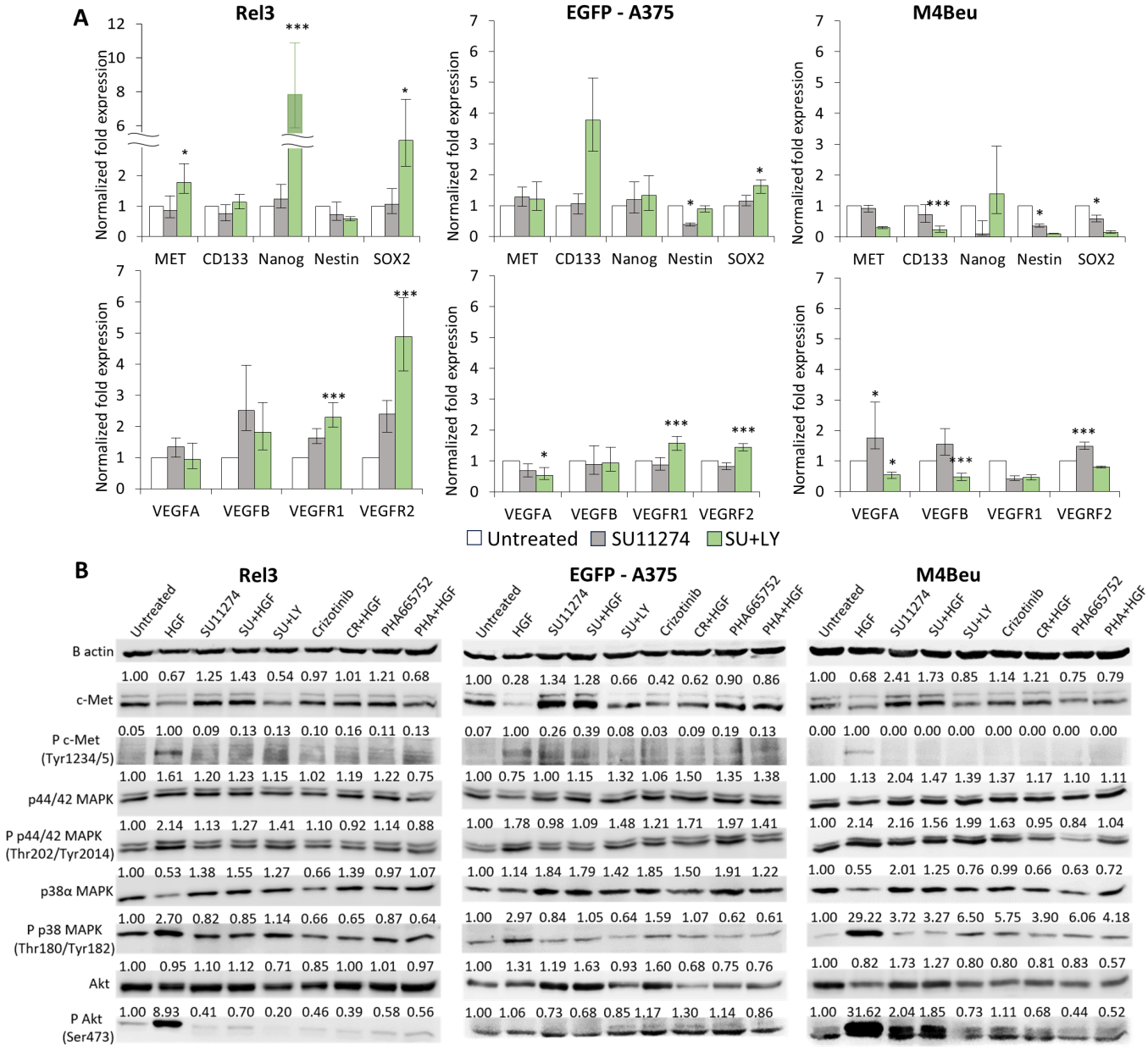

Figure 2. Changes in gene expression induced by combination treatment with SU11274 and LY294002 in Rel3, EGFP-A375, and M4Beu cell lines. A) The normalized expression of CSC and pluripotency markers and gene expression of the factors and receptors of vascularization and angiogenesis after treatment with SU+LY. The gene expression in all three cell lines was normalized to housekeeping genes *ACTB* and *HPRT1*: *p<0.05 and ***p<0.001. B) Intracellular signaling via HGF/c-Met pathway. The cells were exposed to SU11274, SU+LY, crizotinib, and PHA665752 for 24 h. The protein signal was normalized to β-actin, and untreated Rel3 cells were set as a control. The phospho-c-Met 1234/1235 was normalized to β-actin, and the HGF-stimulated Rel3 cells were used as the positive control.

We utilize the lung colonization assay to observe the metastatic potential of Rel3 cells. To mimic long-term treatment, we exposed the cells to the inhibitor for seven days to observe if their aggressive behavior changed compared to untreated cells. Two groups of four mice were injected *iv* into the tail vein with 1×10^6 Rel3 or SU11274-Rel3 cells. We used qPCR to detect the expression of the EGFP gene in the mice's lungs and metastasis as a marker for the presence of Rel3 cells. The graph (Figure 3B) displays insignificant differences in EGFP expression levels between mice injected with untreated Rel3 cells and those injected with SU11274-Rel3 cells. Healthy mouse lungs were used as negative controls, and Rel3 cells were used as positive controls. Mice injected *iv* with Rel3 cells did not exhibit visible infiltration of the lymph nodes (0/4), and the tumor foci were not visible in the lung parenchyma. During the necropsy, we found more extensive lung metas-

tasis infiltration in the SU11274-Rel3 mice group with visible tumor foci in the lung parenchyma (Figure 3C). Lymph node metastasis was observed in this group, causing anatomical shifts in the thoracic cavity of two animals (2/4) (Figure 3D). The metastatic potential of Rel3 cells was not reduced by the *in vitro* pretreatment with the inhibitor SU11274.

Discussion

Our earlier research revealed a decreased proliferation of melanoma cells in both adherent and spheroid cultures following treatment with c-Met inhibitor SU11274. However, intriguingly, we observed an augmented metastatic potential and an increase in melanoma-initiating *in vivo* cells subsequent to SU11274 treatment [14]. In the present study, we investigated the impact of three c-Met inhibitors-SU11274, crizotinib, and PHA665752, and the combination of SU11274 with LY29004, an effective inactivator of PI3K and AKT proteins, on molecular characteristics, tumorigenicity, and metastatic behavior of human melanoma cell lines, differing in their metastatic potential. Initially, we focused on evaluating the treatment-induced expression of putative melanoma CSC, pluripotency, and angiogenic markers and their modulation after exposure to c-Met inhibitors. While SU11274 exposure did not increase CSC markers, we observed upregulation of *MET, CD133*, and *Nanog* genes in Rel3 cells following treatment with crizotinib and PHA665752. SU11274 treatment was not associated with any significant alteration in the expression of CSC markers in EGFP-A375 cells. Conversely, SU11274 significantly decreased the expression of *Nestin* and *SOX2* in M4Beu cells. A similar experimental setup with SU11274 and crizotinib was reported for glioblastoma. The authors reported that SU11274 significantly reduced the proportion of *CD133*-positive cells and showed that it inhibits *Nestin* and *SOX2* gene expression. Similar effects were observed in response to another specific c-Met inhibitor, crizotinib [12]. Melanocytes, pigment-producing cells, arise from the neural crest and migrate to their final destinations in the skin, uveal tract, meninges, and mucosa [19]. The intermediate filament *Nestin*, a neural stem-cell marker, is expressed higher in melanomas than benign melanocytic lesions and is increasingly expressed in advanced melanoma stages. Notably, strong expression of *Nestin* was significantly associated with reduced survival in multivariate analysis, and increased *Nestin* expression was related to aggressive melanoma features. *Nestin* was expressed to varying degrees in most nodular melanomas (92%). It was strongly associated with increased tumor thickness, high mitotic count, ulceration, and tumor necrosis [20]. In another study, *Nestin* was overexpressed in metastatic lesions. Part of the metastases was either *Nestin* negative or mildly positive, but there was no direct association between the lesions with higher concentrations of *Nestin* and poorer prognosis. In patients with positive sentinel lymph nodes, primary tumors were both *Nestin* negative and *Nestin* positive [21].

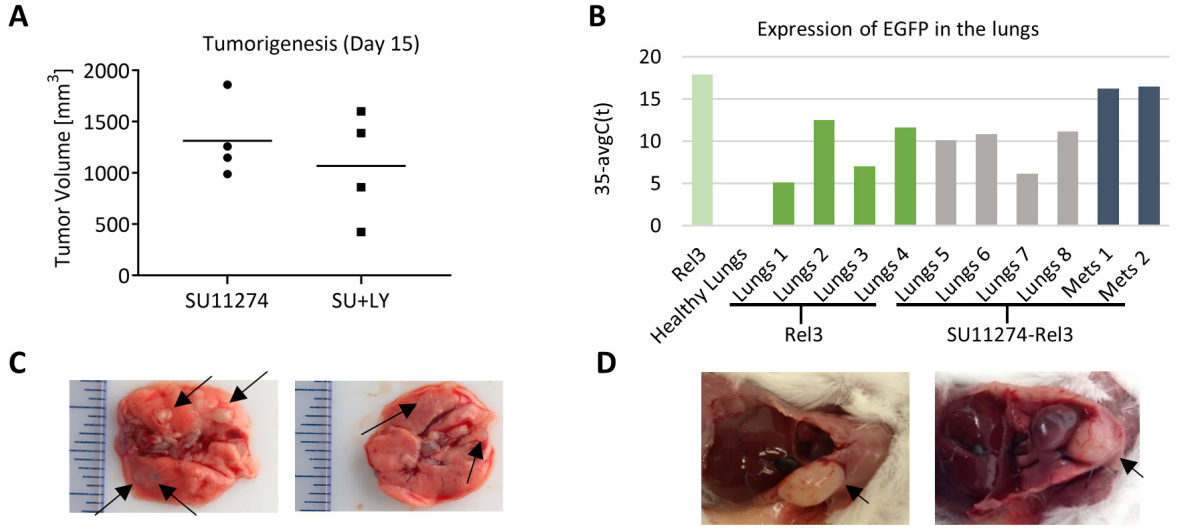

Figure 3. Tumorigenic and metastatic potential of pretreated Rel3 cells *in vivo*. A) Subcutaneous tumor growth of the Rel3 cells was pretreated with 1 μM SU11274 (n=4) and a combination of 1 μM SU11274 and 1 μM LY29004 (n=4). The graph illustrates each group's average tumor volume [mm³] until day 15. There is no significant difference between the groups. B) Mice were injected IV into the tail vein with untreated Rel3 and 1 μM SU11274 pretreated Rel3 cells (7 days). The graph depicts the variation in *EGFP* expression levels in lungs with metastasis relative to negative controls (healthy mouse lung) and in lymph node metastasis. *EGFP* gene expression was quantified using qPCR; Rel3 cells were used as a positive control for *EGFP* expression. C) Pictures show massive metastasis infiltration on the ventral and dorsal sides, and the surface of the lungs has a bumpy appearance, as indicated by the arrows. D) Lymph node metastasis infiltration. The first metastasis grew subcutaneously in the left side of the thorax wall. The second metastasis was located cranially from the heart base in the pleural cavity, and the heart was pushed to the right. C, D) pictures are from the SU11274-Rel3 mouse group

The increased expression of *CD166*, *CD133*, and *Nestin* in melanoma suggests that progression to malignant melanoma likely involves genetic pathways crucial to stem cell biology and normal tissue development [22]. *Nestin* and *SOX2,* stem cell transcription factors that bind an enhancer region on the *Nestin* gene, are preferentially co-expressed in metastatic melanomas compared with nevi or primary melanomas. Moreover, *SOX2*-positive melanoma cells tend to be more spindle-shaped, and they have a more peripheral *Nestin* pattern, which may represent a motile, more mesenchymal phenotype. Such preliminary observations suggest a possible role for *Nestin* and *SOX2* in melanoma metastasis and epithelial-to-mesenchymal transition [23, 24]. The results of Santini et al. indicate that *SOX2* regulates self-renewal and promotes the survival of melanoma-initiating cells [25]. Elevated *SOX2* expression might play an essential role in the high metastatic potential of SU11274 pretreated Rel3 cells.

The receptors for *VEGF*, *VEGFR1,* and *VEGFR2* are members of the RTK family. The VEGFs, VEGFRs, are believed to be significant drivers of tumor angiogenesis, which play essential roles in tumor malignancy (such as sustaining tumor growth) and in blood-borne metastasis [26, 27]. Many studies showed the vascular system is crucial to metastasis. Therefore, the effects of various antiangiogenic therapies are still being investigated in preclinical and clinical trials. Resistance to anti-VEGF monotherapy was observed in malignant melanoma [28]. The study by Redondo et al. showed that melanoma cells produce increased *VEGF* concentrations *in vitro*, and *VEGF* concentrations were increased in patients with primary melanoma, patients with local recurrence, and highest in metastatic melanoma in contrast to the healthy controls [29]. Our results demonstrated that crizotinib and PHA665752 elevated *VEGFA, VEGFB* and *VEGFR1, VEGFR2* in Rel3 cells and increased the potential of angiogenesis in tumorigenesis. Our findings contrast with the study by Cozzo et al., who showed that crizotinib disrupted tumor vascularization in an animal study of breast cancer [30]. These data indicate tumor-specific response to the treatment by small molecule inhibitor and, more importantly, illustrate the adaptive reactions of highly plastic melanoma cells to the inhibitory treatment. In the study by Surriga et al., authors treated mice with crizotinib starting one week after uveal melanoma metastatic cells were transplanted. They observed a significant reduction in the development of metastases as compared with untreated controls [31].

The MAPK and Akt pathways are the most mutated signaling pathways in human cancers and common targets for anticancer therapies. More than 50% of tumors carry the BRAF V600E mutation in malignant melanoma, and 70% have increased Akt phosphorylation and may have activated mTOR signaling [32]. LY294002 is a potent inhibitor of numerous proteins. It is generally considered a non-selective inhibitor for PI3K and is widely used to inhibit the PI3K/AKT pathway [33]. Inhibition of PI3K inhibits the early phase of melanoma cell transmigration after treatment by inhibitor LY294002. It was reported that in the A375 melanoma cells, which presented a rounded morphology during adhesion, the number of adherent cells was significantly reduced after adding LY294002 [34]. Also, it was discovered that LY294002 significantly reduced the phosphorylation of Akt in melanoma cell line WM983A [35], and LY294002 treatment decreases the invasion and migration of melanoma cell lines Skmel28, 501mel (human melanoma cell lines), and B16 (mouse melanoma cell line) [36]. We focused on survival and cell migration changes via inhibiting the HGF/c-Met signaling pathway through combination treatment. We noticed a similar inhibition effect in our experiments but could not reduce or completely inhibit phosphorylation on Akt, p44/42, and p38 MAPKs using c-Met inhibitors. This may be because oncogene BRAF is also constitutively activated in the EGFP-A375 and Rel3 cells [37]. The BRAF V600E mutation leads to the constitutive activation of the MAPK pathway, and the suppression of Akt activation in melanoma is probably mediated by overactive MAPK signaling [32]. However, this contradicts our results because Akt (Ser473) was phosphorylated in BRAF-mutated cells EGFP-A375, and the phosphorylation remained high despite treatment. Another study showed four different c-Met inhibitors, SU11274, PHA665752, EMD1214063, and PF02341066, which efficiently inhibit c-Met autophosphorylation at kinase tyrosines 1234/1235 in five out of seven cell lines, that concomitant treatment increased total c-Met levels in a dose-dependent manner [38]. We noticed a similar result and tendency in hypermetastatic melanoma Rel3 cells after the treatment with c-Met inhibitors, which inhibited phosphorylation on tyrosine 1234/1235 and increased the total level of c-Met protein and its expression.

We examined whether the drugs inhibited c-Met and the downstream signaling pathways, and we noticed insufficient inhibition of phosphorylation after treatment with SU11274, crizotinib, PHA665752, and SU+LY. These results partially correlate with the findings of Surriga et al. Their study revealed that crizotinib could not effectively inhibit the phosphorylation of its target kinases, including p-ALK and p-ROS1, in uveal melanoma. Furthermore, downstream signaling components such as p-Akt, p-ERK, and p-STAT3 showed unchanged levels, indicating limited impact on these key signaling pathways despite crizotinib treatment [39]. Our study demonstrated the specific impact of c-Met inhibitors on melanoma cells, assessing both their tumorigenic potential and the reduced metastatic capacity of pretreated cells. This provided a comprehensive understanding of the c-Met pathway's inhibition. We identified molecular targets affected by c-Met inhibition and explored potential receptor-tyrosine kinase crosstalk related to cell tumorigenicity. However, we observed that the pressure of the inhibitors led to the upregulation of certain CSC markers, which may increase tumorigenicity and reduce the effectiveness of tumor suppression. On the other hand, we found during

the autopsy that SU-pretreated cells formed visibly fewer metastases. The clinical use of these compounds remains limited due to their non-specific action, which can enhance the invasive behavior of melanoma cells. It was found that two weeks after stopping crizotinib treatment, mice previously treated with the drug showed traces of liver metastasis, significantly less than control mice. This suggests metastatic disease's dependence on c-Met signaling. Crizotinib seems to prevent cells from migrating to dominant visceral sites like the liver rather than killing microscopic metastases [8]. This aligns with the lack of single-agent efficacy in our *in vitro* and *in vivo* experiments. The major indications for systemic therapy of metastatic melanoma disease are inoperable regional metastases and distant metastases. From the long list of available cytostatic drugs used for chemotherapy or targeted therapies and immunotherapies, only a few have been able to induce tumor responses in the clinical setting [40]. The clinical application of kinase inhibitors and anti-VEGF antibodies to stop tumor angiogenesis was validated as a therapeutic strategy by positive clinical results with bevacizumab, sorafenib, sunitinib, and pazopanib [41].

In summary, our study underlines the tumor-specific responses to small-molecule inhibitors that, despite inhibiting their target, produce multiple alterations in the tumor cells. This paradoxically may lead to higher tumorigenicity and metastatic potential despite promising antiproliferative effects *in vitro*. Based on our results, we suggest that to achieve antitumorigenic and antimetastatic effects in melanoma, targeting the c-Met receptor is necessary in combination with VEGF antagonists and VEGF receptor inhibitors or agents interfering with CSC markers. The ability of c-MET inhibitors to modulate various pathways involved in the progression and spread of melanoma cells suggests that they could play a crucial role in developing more effective treatments for this aggressive form of cancer.

Supplementary information is available in the online version of the paper.

Acknowledgments: We thank L. Rojikova, M. Dubrovcakova, A. Linekova, and E. Novakova for their excellent technical assistance. This work was supported by the Slovak Research and Development Agency under the contract No. APVV-17-0369, by the VEGA grant No. 1/0395/21, and Stefan Schwarz Support Fund. The experiments mentioned in the study were enabled with the kind help and financial support from the Slovak Cancer Research Foundation and League against Cancer.

References

[1] LIM YC, KANG HJ, MOON JH. C-Met pathway promotes self-renewal and tumorigenecity of head and neck squamous cell carcinoma stem-like cell. Oral Oncol 2014; 50: 633–639. https://doi.org/10.1016/j.oraloncology.2014.04.004

[2] CAO HH, CHENG CY, SU T, FU XQ, GUO H et al. Quercetin inhibits HGF/c-Met signaling and HGF-stimulated melanoma cell migration and invasion. Mol Cancer 2015; 14: 103. https://doi.org/10.1186/s12943-015-0367-4

[3] CZYZ M. HGF/c-MET Signaling in Melanocytes and Melanoma. Int J Mol Sci 2018; 19: 3844. https://doi.org/10.3390/ijms19123844

[4] GARAJOVÁ I, GIOVANNETTI E, BIASCO G, PETERS GJ. c-Met as a Target for Personalized Therapy. Transl Oncogenomics 2015; 7: 13–31. https://doi.org/10.4137/tog.s30534

[5] SABBAH M, NAJEM A, KRAYEM M, AWADA A, JOURNE F et al. RTK Inhibitors in Melanoma: From Bench to Bedside. Cancers (Basel) 2021; 13: 1685. https://doi.org/10.3390/cancers13071685

[6] CAO HH, TSE AKW, KWAN HY, YU H, CHENG CY et al. Quercetin exerts anti-melanoma activities and inhibits STAT3 signaling. Biochem Pharmacol 2014; 87: 424–434. https://doi.org/10.1016/j.bcp.2013.11.008

[7] CHATTOPADHYAY C, ELLERHORST JA, EKMEKCIOGLU S, GREENE VR, DAVIES MA et al. Association of activated c-Met with NRAS-mutated human melanomas. Int J Cancer 2012; 131: E56–65. https://doi.org/10.1002/ijc.26487

[8] SURRIGA O, RAJASEKHAR VK, AMBROSINI G, DOGAN Y, HUANG R et al. Crizotinib, a c-Met inhibitor, prevents metastasis in a metastatic uveal melanoma model. Mol Cancer Ther 2013; 12: 2817–2826. https://doi.org/10.1158/1535-7163.Mct-13-0499

[9] SUN C, WANG L, HUANG S, HEYNEN GJJE, PRAHALLAD A et al. Reversible and adaptive resistance to BRAF(V600E) inhibition in melanoma. Nature 2014; 508: 118–122. https://doi.org/10.1038/nature13121

[10] LI FZ, DHILLON AS, ANDERSON RL, MCARTHUR G, FERRAO PT. Phenotype switching in melanoma: implications for progression and therapy. Front Oncol 2015; 5: 31. https://doi.org/10.3389/fonc.2015.00031

[11] KENESSEY I, KESZTHELYI M, KRAMER Z, BERTA J, ADAM A et al. Inhibition of c-Met with the Specific Small Molecule Tyrosine Kinase Inhibitor SU11274 Decreases Growth and Metastasis Formation of Experimental Human Melanoma. Curr Cancer Drug Targets 2010; 10: 332–342. https://doi.org/10.2174/156800910791190184

[12] LI Y, LI A, GLAS M, LAL B, YING M et al. c-Met signaling induces a reprogramming network and supports the glioblastoma stem-like phenotype. Proc Natl Acad Sci U S A 2011; 108: 9951–9956. https://doi.org/10.1073/pnas.1016912108

[13] DAS I, WILHELM M, HÖIOM V, FRANCO MARQUEZ R, COSTA SVEDMAN F et al. Combining ERBB family and MET inhibitors is an effective therapeutic strategy in cutaneous malignant melanoma independent of BRAF/NRAS mutation status. Cell Death & Disease 2019; 10: 663. https://doi.org/10.1038/s41419-019-1875-8

[14] KUCEROVA L, DEMKOVA L, SKOLEKOVA S, BOHOVIC R, MATUSKOVA M. Tyrosine kinase inhibitor SU11274 increased tumorigenicity and enriched for melanoma-initiating cells by bioenergetic modulation. BMC Cancer 2016; 16: 308. https://doi.org/10.1186/s12885-016-2341-y

[15] KUCEROVA L, SKOLEKOVA S, DEMKOVA L, BOHOVIC R, MATUSKOVA M. Long-term efficiency of mesenchymal stromal cell-mediated CD-MSC/5FC therapy in human melanoma xenograft model. Gene Ther 2014; 21: 874–887. https://doi.org/10.1038/gt.2014.66

[16] KUCEROVA L, MATUSKOVA M, PASTORAKOVA A, TYCIAKOVA S, JAKUBIKOVA J et al. Cytosine deaminase expressing human mesenchymal stem cells mediated tumour regression in melanoma bearing mice. J Gene Med 2008; 10: 1071–1082. https://doi.org/10.1002/jgm.1239

[17] PFAFFL MW, HORGAN GW, DEMPFLE L. Relative expression software tool (REST©) for group-wise comparison and statistical analysis of relative expression results in real-time PCR. Nucleic Acids Res 2002; 30: e36–e36. https://doi.org/10.1093/nar/30.9.e36

[18] TOMAYKO MM, REYNOLDS CP. Determination of subcutaneous tumor size in athymic (nude) mice. Cancer Chemother Pharmacol 1989; 24: 148–154. https://doi.org/10.1007/BF00300234

[19] KOZOVSKA Z, GABRISOVA V, KUCEROVA L. Malignant melanoma: diagnosis, treatment and cancer stem cells. Neoplasma 2016; 63: 510–517. https://doi.org/10.4149/neo_2016_403

[20] LADSTEIN RG, BACHMANN IM, STRAUME O, AKSLEN LA. Nestin expression is associated with aggressive cutaneous melanoma of the nodular type. Modern Pathology 2013; 27: 396. https://doi.org/10.1038/modpathol.2013.151

[21] BRYCHTOVA S, FIURASKOVA M, HLOBILKOVÁ A, BRYCHTA T, HIRNAK J. Nestin expression in cutaneous melanomas and melanocytic nevi. J Cutan Pathol 2007; 34: 370–375. https://doi.org/10.1111/j.1600-0560.2006.00627.x

[22] KLEIN WM, WU BP, ZHAO S, WU H, KLEIN-SZANTO AJP et al. Increased expression of stem cell markers in malignant melanoma. Mod Pathol 2006; 20: 102. https://doi.org/10.1038/modpathol.3800720

[23] GIROUARD SD, MURPHY GF. Melanoma stem cells: not rare, but well done. Lab Invest 2011; 91: 647. https://doi.org/10.1038/labinvest.2011.50

[24] LAGA AC, ZHAN Q, WEISHAUPT C, MA J, FRANK MH et al. SOX2 and nestin expression in human melanoma: an immunohistochemical and experimental study. Exp Dermatol 2011; 20: 339–345. https://doi.org/10.1111/j.1600-0625.2011.01247.x

[25] SANTINI R, PIETROBONO S, PANDOLFI S, MONTAGNANI V, D'AMICO M et al. SOX2 regulates self-renewal and tumorigenicity of human melanoma-initiating cells. Oncogene 2014; 33: 4697–4708. https://doi.org/10.1038/onc.2014.71

[26] LEMMON MA, SCHLESSINGER J. Cell Signaling by Receptor Tyrosine Kinases. Cell 2010; 141: 1117–1134. https://doi.org/10.1016/j.cell.2010.06.011

[27] SHIBUYA M, CLAESSON-WELSH L. Signal transduction by VEGF receptors in regulation of angiogenesis and lymphangiogenesis. Exp Cell Res 2006; 312: 549–560. https://doi.org/10.1016/j.yexcr.2005.11.012

[28] FELCHT M, THOMAS M. Angiogenesis in malignant melanoma. J Dtsch Dermatol Ges 2015; 13: 125–135. https://doi.org/10.1111/ddg.12580

[29] REDONDO P, BANDRÉS E, SOLANO T, OKROUJNOV I, GARCÍA-FONCILLAS J. Vascular endothelial growth factor (VEGF) and melanoma. N-acetylcysteine downregulates VEGF production in vitro. Cytokine 2000; 12: 374–378. https://doi.org/10.1006/cyto.1999.0566

[30] COZZO AJ, SUNDARAM S, ZATTRA O, QIN Y, FREEMERMAN AJ et al. cMET inhibitor crizotinib impairs angiogenesis and reduces tumor burden in the C3(1)-Tag model of basal-like breast cancer. Springerplus 2016; 5: 348–348. https://doi.org/10.1186/s40064-016-1920-3

[31] SURRIGA O, RAJASEKHAR VK, AMBROSINI G, DOGAN Y, HUANG R et al. Crizotinib, a c-Met Inhibitor, Prevents Metastasis in a Metastatic Uveal Melanoma Model. Mol Cancer Ther 2013; 12: 2817. https://doi.org/10.1158/1535-7163.mct-13-0499

[32] CHEN B, TARDELL C, HIGGINS B, PACKMAN K, BOYLAN JF et al. BRAFV600E Negatively Regulates the AKT Pathway in Melanoma Cell Lines. PLoS One 2012; 7: e42598. https://doi.org/10.1371/journal.pone.0042598

[33] GHARBI SI, ZVELEBIL MJ, SHUTTLEWORTH SJ, HANCOX T, SAGHIR N et al. Exploring the specificity of the PI3K family inhibitor LY294002. Biochem J 2007; 404: 15–21. https://doi.org/10.1042/bj20061489

[34] MOLNÁR J, FAZAKAS C, HASKÓ J, SIPOS O, NAGY K et al. Transmigration characteristics of breast cancer and melanoma cells through the brain endothelium: Role of Rac and PI3K. Cell Adh Migr 2016; 10: 269–281. https://doi.org/10.1080/19336918.2015.1122156

[35] SHAO H, WELLS A. Deciphering the molecular mechanism of enhanced tumor activity of the EGFR variant T790M/L858R using melanoma cell lines. Front Oncol 2023; 13: 1163504. https://doi.org/10.3389/fonc.2023.1163504

[36] BONVIN E, FALLETTA P, SHAW H, DELMAS V, GODING CR. A phosphatidylinositol 3-kinase-Pax3 axis regulates Brn-2 expression in melanoma. Mol Cell Biol 2012; 32: 4674–4683. https://doi.org/10.1128/mcb.01067-12

[37] SINI MC, DONEDDU V, PALIOGIANNIS P, CASULA M, COLOMBINO M et al. Genetic alterations in main candidate genes during melanoma progression. Oncotarget 2018; 9: 8531–8541. https://doi.org/10.18632/oncotarget.23989

[38] LEISER D, POCHON B, BLANK-LISS W, FRANCICA P, GLÜCK AA et al. Targeting of the MET receptor tyrosine kinase by small molecule inhibitors leads to MET accumulation by impairing the receptor downregulation. FEBS Letters 2014; 588: 653–658. https://doi.org/10.1016/j.febslet.2013.12.025

[39] SURRIGA O, RAJASEKHAR VK, AMBROSINI G, DOGAN Y, HUANG R et al. Crizotinib, a c-Met Inhibitor, Prevents Metastasis in a Metastatic Uveal Melanoma Model. Mol Cancer Ther 2013; 12: 2817–2826. https://doi.org/10.1158/1535-7163.mct-13-0499

[40] GARBE C, PERIS K, HAUSCHILD A, SAIAG P, MIDDLETON M et al. Diagnosis and treatment of melanoma. European consensus-based interdisciplinary guideline – Update 2016. Eur J Cancer 2016; 63: 201–217. https://doi.org/10.1016/j.ejca.2016.05.005

[41] HUDKINS RL, BECKNELL NC, ZULLI AL, UNDERINER TL, ANGELES TS et al. Synthesis and Biological Profile of the pan-Vascular Endothelial Growth Factor Receptor/Tyrosine Kinase with Immunoglobulin and Epidermal Growth Factor-Like Homology Domains 2 (VEGF-R/TIE-2) Inhibitor 11-(2-Methylpropyl)-12,13-dihydro-2-methyl-8-(pyrimidin-2-ylamino)-4H-indazolo[5,4-a]pyrrolo[3,4-c]carbazol-4-one (CEP-11981): A Novel Oncology Therapeutic Agent. Journal of Medicinal Chemistry 2012; 55: 903–913. https://doi.org/10.1021/jm201449n

https://doi.org/10.4149/neo_2024_240523N232

The impact of c-Met inhibition on molecular features and metastatic potential of melanoma cells

Lucia DEMKOVA[1,*], Miroslava MATUSKOVA[1], Katarina GERCAKOVA[1], Zuzana KOZOVSKA[1], Bozena SMOLKOVA[1], Lucia KUCEROVA[1,2]

Supplementary Information

Supplementary Table S1. Primers Sequences used for qPCR.

Primer symbol	Forward 5`–3`	Revers 5`–3`	Product length bp
HPRT1	TGACCAGTCAACAGGGGACA	ACTGCCTGACCAAGGAAAGC	136
GAPDH	GAAGGTGAAGGTCGGAGTC	GAAGATGGTGATGGGATTTC	226
ACTB	GGACTTCGAGCAAGAGATGG	AGCACTGTGTTGGCGTACAG	235
MET	CAGATGTGTGGTCCTTTG	ATTCGGGTTGTAGGAGTCT	129
CD133	TGGATGCAGAACTTGACAACGT	ATACCTGCTACGACAGTCGTGGT	133
Nanog	CAAAGGCAAACAACCCACTT	ATTGTTCCAGGTCTGGTTGC	346
Nestin	AGCCCTGACCACTCCAGTTTAG	CCCTCTATGGCTGTTTCTTTCTCT	128
SOX2	GGAAAGTTGGGATCGAACAA	GCGAACCATCTCTGTGGTCT	145
VEGFA	AGCTGCGCTGATAGACATCC	CTACCTCCACCATGCCAAGT	104
VEGFB	GGCTTCACAGCACTGTCCTT	AAGTCCGGATGCAGATCCT	116
VEGFR1	GGCGAACGAGAGGACGGACT	GCATGATGTGCTGGGTGCCT	216
VEGFR2	ATCAGAGTGGCAGTGAGCAAAGGG	CAAGTCAGTTTCCCGGTAGAAGCAC	134
GFP	CTCGTGACCACCCTGACCTA	TCGCCCTCGAACTTCACCTC	173

Supplementary Table S2. Primary and secondary antibodies used for western blotting.

Antibodies	CN#	Species/Isotype	MW (kDa)	Dilutions	Dilute in	Company
Akt1, Akt2, Akt3	9272	Rabbit/IgG	60	1:2000	5% BSA	CST
Phospho-Akt (Ser473)	9271	Rabbit/IgG	60	1:2000	5% BSA	CST
Met (D1C2) XP	8198	Rabbit/IgG	140, 170	1:1000	5% MILK	CST
Phospho-Met (Tyr1234/1235)	3129	Rabbit/IgG	170	1:500	5% BSA	CST
p38α MAP Kinase	9228	Rabbit/IgG	40	1:2000	5% BSA	CST
Phospho-p38 MAP Kinase (Thr180/Tyr182)	4092	Rabbit/IgG	43	1:2000	5% BSA	CST
p44/42 Mapk (Erk1/2)	4695	Rabbit/IgG	44/42	1:2000	5% BSA	CST
Phospho-p44/42 Mapk (Erk1/2) (Thr202/Tyr204)	4370	Rabbit/IgG	44/42	1:2000	5% BSA	CST
Anti-β-Actin	A2228	Mouse/IgG	42	1:2000-1:4000	5% MILK	Sigma-Aldrich
Goat polyclonal anti-rabbit IgG, HRP-linked	7074	Rabbit/IgG secondary antibody		1:1000-1:3000	0.1% TBST	CST
Goat anti-Mouse IgG (H+L) highly cross-adsorbed, Alexa Fluor 680	6721	Mouse/IgG secondary antibody		1:10000	0.1% TBST	Thermo Scientific